



**Discover Generics**

Cost-Effective CT & MRI Contrast Agents

 **FRESENIUS  
KABI**

[WATCH VIDEO](#)

**AJNR**

## **MR Imaging of Experimental Demyelination**

Louis M. Teresi, David Hovda, Allen B. Seeley, Katherine Nitta  
and Robert B. Lufkin

*AJNR Am J Neuroradiol* 1989, 10 (2) 307-314  
<http://www.ajnr.org/content/10/2/307>

This information is current as  
of June 1, 2025.

## MR Imaging of Experimental Demyelination

Louis M. Teresi<sup>1</sup>  
 David Hovda  
 Allen B. Seeley  
 Katherine Nitta  
 Robert B. Lufkin

Seventeen rabbit sciatic nerves undergoing experimental demyelination and 17 control nerves were imaged *in vivo* with a 0.3-T MR imaging system using a silicone chamber wrapped around the nerves to isolate them from surrounding tissues. Three pulse sequences were used for each nerve: (1) spin-echo 500/28 (TR/TE), (2) spin-echo 2000/56, and (3) inversion recovery 1000/300/30 (TR/TI/TE). Image intensity data were acquired for each nerve by placing a region of interest over the nerve and measuring pixel brightness within the region of interest by means of a computer algorithm. The mean signal intensity of the experimental nerve was then compared with the mean signal intensity of the contralateral control nerve on the same image. Histologic sections of the nerves were stained with Loyez's stain for myelin and thionin for glial cells. MR findings were then compared with histopathologic data. Experimental nerves showed distinct stages of demyelination. Two fundamental observations were surmised from the data: (1) Perceptible MR signal changes are associated with early nerve degeneration, in which there is demyelination in the absence of glial cell proliferation; these changes are appreciated as increased intensity on heavily T2-weighted sequence. In these nerves no signal changes are seen on T1-weighted sequences. (2) Perceptible MR signal changes are associated with more advanced nerve degeneration, in which there is an increase in the number of glial cells in the absence of further demyelination; these changes are appreciated as decreased intensity on T1-weighted sequences and markedly increased intensity on T2-weighted sequences, respectively.

The results show that MR can distinguish stages of demyelination in degenerating nerves, thereby providing a powerful method for the diagnosis and characterization of demyelinating disease.

The process of demyelination is common to many neurologic diseases in both the central and peripheral nervous systems. MR imaging has shown the potential to differentiate between myelinated and demyelinated nerves and to identify focal lesions in demyelinating disease, such as multiple sclerosis [1–5]. Early studies of demyelination associated with wallerian degeneration have suggested that T1 and T2 values lengthen in this disease process [2, 4]. A limitation of the experimental design used in these studies is that MR data were acquired with a spectrometer, not an imager, without consideration for the cumulative effects of T1, T2, and proton-density data on image signal for a given pulse sequence. Thus, the cumulative effect of changes in proton-density and T1 and T2 values on the resulting signal, as observed on MR routinely generated in the clinical environment, is as yet poorly understood. Determining the MR signal changes associated with the evolving histologic stages of nerve demyelination would contribute significantly to our understanding of the sensitivity and specificity of MR signal changes seen in clinically suspected demyelination in both the central and peripheral nervous systems.

To date, no experimental model of nerve demyelination has allowed direct correlation of histopathologic and MR image data. We developed an animal model, the "silicone chamber model," that allows us to image isolated sciatic nerves in

This article appears in the March/April 1989 issue of *AJNR* and the June 1989 issue of *AJR*.

Received March 9, 1988; accepted after revision November 1, 1988.

Presented at the annual meeting of the American Roentgen Ray Society, San Francisco, CA, May 1988. Recipient of the ARRS Executive Council Award.

<sup>1</sup> All authors: Department of Radiological Sciences, University of California, Los Angeles, School of Medicine, UCLA Medical Center, BL-428, Los Angeles, CA 90024. Address reprint requests to L. M. Teresi.

*AJNR* 10:307–314, March/April 1989  
 0195–6108/89/1002–0307  
 © American Society of Neuroradiology

vivo and to readily compare MR findings with histopathologic data. We report the signal changes on MR associated with the progressively more severe histologic stages of demyelination as observed in this unique experimental model.

## Materials and Methods

Thirty-four sciatic nerves in 17 large (5–6 kg) adult male New Zealand white rabbits\* were studied. After induction of general anesthesia with approximately 1 ml/kg IV thiamylal sodium† titrated to effect, both right and left sciatic nerves were gently dissected from surrounding tissues. In each rabbit, the left sciatic nerve was subjected to experimental demyelination, while the right sciatic nerve served as a control. Experimental demyelination was induced by three methods: (1) crush injury, (2) transection, and (3) exposure to pure alcohol. In seven rabbits, the nerve was crushed with forceps at the level of the sciatic notch, while in five rabbits the nerve was transected with a scalpel at the level of the sciatic notch. In five rabbits the experimental nerve was bathed in a solution of 100% isopropyl alcohol for 3 min. In each rabbit, the contralateral control nerve, although dissected from surrounding tissues, was not manipulated further. The surgical wounds on both the experimental and control sides were then irrigated with isotonic normal saline solution and closed. The animals were then allowed full activity. All rabbits were imaged 14 days after induction of experimental demyelination.

Immediately before imaging, general anesthesia was again induced with IV Surital, and both right (control) and left (experimental) sciatic nerves were gently dissected from surrounding tissues. Each nerve was then inserted into a silicone tube measuring 7 mm in external diameter, 5 mm internal diameter, and 4 cm in length that had been cut along its long axis on a single side (Fig. 1A). The nerve was therefore isolated from surrounding soft tissues within the silicone tube. The surgical wounds on both the experimental and control sides were then irrigated with isotonic normal saline solution and closed. While still under general anesthesia, the rabbit was transferred from the surgical suite to the MR suite for imaging. General anesthesia was continued through the imaging protocol to prevent motion.

Imaging was performed on a 0.3-T hybrid magnet imaging system.‡ The rabbit was positioned on its side in the scanner gantry such that the thighs of the animal were oriented perpendicular to the long axis of the gantry. A solenoid surface receiver coil was then wrapped around the lower extremities. First, a seven-slice axial T1-weighted spin-echo (SE) scout image, SE 500/28/1 (TR/TE/excitations), was obtained. With the rabbit positioned in the gantry in this manner, the axial scout sequence generally would produce an image of the length of the silicone chambers in the rabbit's thighs (Fig. 1B). If the scout image did not provide a satisfactory image of the length of the silicone chambers, the rabbit was repositioned and a second axial scout image was obtained (Fig. 1B).

Using the axial scout image, we then positioned cursor lines across the length of the silicone chambers and obtained three further imaging sequences: (1) SE 500/28/2–4, (2) SE 2000/56/2, and (3) inversion-recovery (IR) 1000/300/30/2 (TR/TI/TE/excitations). In all sequences 5-mm-thick sections with a 2-mm interslice gap were used. All sequences were obtained in precisely the same location with the same scout cursor line positions. This imaging protocol, therefore, produced three directly comparable multislice 5-mm-thick cross-sectional images of both control and experimental nerves isolated from surrounding tissues by their respective silicone chambers (Fig. 2).

Image intensity data were acquired for each nerve by placing a cursor-guided range of interest over the nerve and measuring pixel

brightness within the region of interest with a computer algorithm. Three independent measurements of the signal intensity of the experimental and control nerves were made from each image. The mean signal intensity of the experimental nerve was then compared with the mean signal intensity of the control nerve on the same image.

After imaging, each nerve was transected flush with the proximal and distal ends of the silicone chamber. This segment of nerve contained within the silicone chamber was then removed from the animal in toto with the silicone chamber and its proximal end marked with a single 5–0 suture. Both the nerve and chamber were then transferred directly to a buffered 10% formalin bath. After this procedure, the animal was sacrificed by lethal IV air embolization.

After being fixed in the formalin bath, each nerve was removed from its respective silicone chamber and imbedded in paraffin. With a standard rotary microtome, 25- $\mu$ m-thick sections were alternately stained with Loyez's stain for myelin (odd sections) and thionin for Nissl bodies, which are present in glial cells (even sections). Respective sections were then examined under light microscopy.

## Results

### Control Nerves

Control nerves appeared as rounded or oval structures of intermediate intensity measuring 2–4 mm in diameter surrounded by a circular area of signal void produced by the silicone chamber when imaged in cross section (Figs. 2A–2C). The signal intensity of control nerves approximated that of muscle on SE 2000/56 and SE 500/28 sequences. On IR 1000/300/30 images, control nerves were slightly more intense than muscle. Myelin and thionin histologic preparations on all control nerves showed intact myelin sheaths and a normal number of glial elements, respectively (Figs. 3A and 3B).

### Experimental Nerves

Review of the myelin and thionin preparations of nerves subjected to experimental demyelination revealed three distinct categories of histologic changes (Table 1): Category 1 was characterized by beading and fragmentation of myelin around most axon cylinders and some axon cylinders showing complete loss of myelin. These changes in myelin were associated with a doubling of glial elements (Figs. 3C and 3D). Category 2 was characterized by further loss of myelin with only scattered myelin fragments present. In these nerves there was no perceptible increase in the number of glial elements compared with category 1 (Figs. 3E and 3F). Category 3 was characterized by no further loss of myelin compared with category 2, but a more than fourfold increase in the number of glial elements compared with control nerves (Figs. 3F and 3G).

Nerves subjected to crush or transection at the level of the sciatic notch showed variable degrees of demyelination and gliosis, depending on the distance along the nerve distal to the site of injury. In general, more demyelination and proliferation of glial elements was observed in the proximal, compared with the distal, portions of these nerves. Nerves exposed to pure alcohol showed more uniform demyelination and gliosis along the course of the nerve. In all nerves exposed to pure alcohol, demyelination was nearly complete (category

\* Irish Farms, Riverside, CA.

† Surital, Parke-Davis, Newark, NJ.

‡ Fonar 3000M, Fonar Corp., Melville, NY.

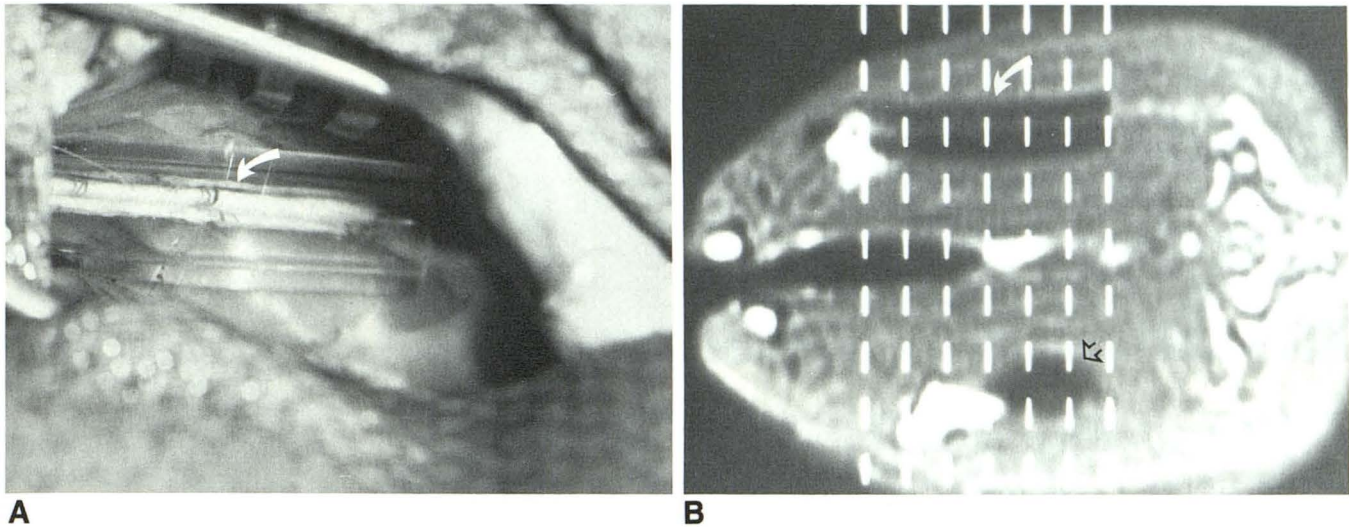


Fig. 1.—A, Intraoperative photograph shows sciatic nerve (arrow) positioned in silicone chamber for imaging. B, SE 500/28. T1-weighted scout image shows length of silicone chamber as low-signal region in leg of rabbit (curved arrow). A small portion of contralateral silicone chamber is seen (open arrow) in other leg on this image, and in its entirety on adjacent slices.

3). Table 2 summarizes the number of nerve segments for each type of injury exhibiting a specific category of histologic changes.

MR images of experimental nerves in each histologic category are shown in Figure 2, and their respective myelin- and thionin-stained histologic sections in Figure 3. Relative signal intensity changes in experimental nerves in each histologic category are summarized in Table 3 and Figure 4. *Relative signal intensity* refers to the mean pixel intensity of the experimental nerve divided by the mean pixel intensity of the control nerve on the same image ( $\text{intensity}_{\text{experimental}} / \text{intensity}_{\text{control}}$ ). Signal intensity values in Table 3 and Figure 4 reflect the mean relative signal intensity of all experimental nerves in a given histologic category plus or minus the absolute range of relative intensity values for all nerves in that category. Of note is that all significant relative signal intensity changes could be appreciated on MR.

Nerves showing category 1 histology evidenced marked increase in signal intensity on the T2-weighted SE 2000/56 sequence, approximately 1.5 times that of respective control nerves. T1-weighted SE 500/28 and IR 1000/300/30 sequences showed no significant signal changes. Nerves showing category 2 histology showed further increase in relative signal intensity on the SE 2000/56 sequence compared with category 1 nerves. Unlike category 1 nerves, category 2 nerves showed a moderate increase in signal intensity on the SE 500/28 sequence. No change in relative signal intensity could be seen on the IR 1000/300/30 sequence for category 2 nerves. Category 3 nerves demonstrated an even further increase in relative signal intensity over category 2 nerves on the SE 2000/56 sequence. Unlike category 2 nerves, category 3 nerves evidenced decreased signal intensity on the IR 1000/300/30 sequence. A slight increase in relative signal intensity was sometimes appreciated on the SE 500/28 sequence for category 3 nerves.

## Discussion

To date the cumulative effect of changes in proton density and T1 and T2 values on the resulting signal in degenerating nerves is as yet poorly understood. By using the silicone chamber model, we were able to directly image isolated sciatic nerves in vivo and directly compare MR images with histopathologic data. Thus, we were able to determine the cumulative MR signal intensity changes associated with progressively more severe histologic stages of nerve demyelination with pulsing sequences routinely used in the clinical environment.

In this study we initiated degeneration in rabbit sciatic nerves by transection, crushing, or local application of a toxic substance. Subsequent nerve degeneration and demyelination associated with these techniques have been well described and may be divided into three stages [6–9].

Early in degeneration (stage 1), usually 0–4 days in the peripheral nervous system, the myelin sheath retracts from the axon at the nodes, leaving a greater area of naked axon. This retraction first affects nodes near the lesion, secondarily spreading peripherally. The region of the nerve distal to the lesion becomes incapable of impulse conduction. The retraction of the myelin sheath is followed by the breakdown of the myelin into the so-called “digestion chambers” or ellipsoids in which the remnants of the axis cylinder disintegrate. In this stage there is physical destruction of myelin, without evidence of chemical degradation. Myelin lipids remain unaltered except for a slight diminution of neutral fat.

Between 4 and 7 days after sectioning (stage 2), neuroglial cells proliferate and surround the digestion chambers. The digestion chambers are gradually resorbed, so that by 30 days after nerve section all remnants of the axis cylinder and myelin sheath have disappeared. In this stage there is chemical destruction of myelin. Each of the myelin lipids (free

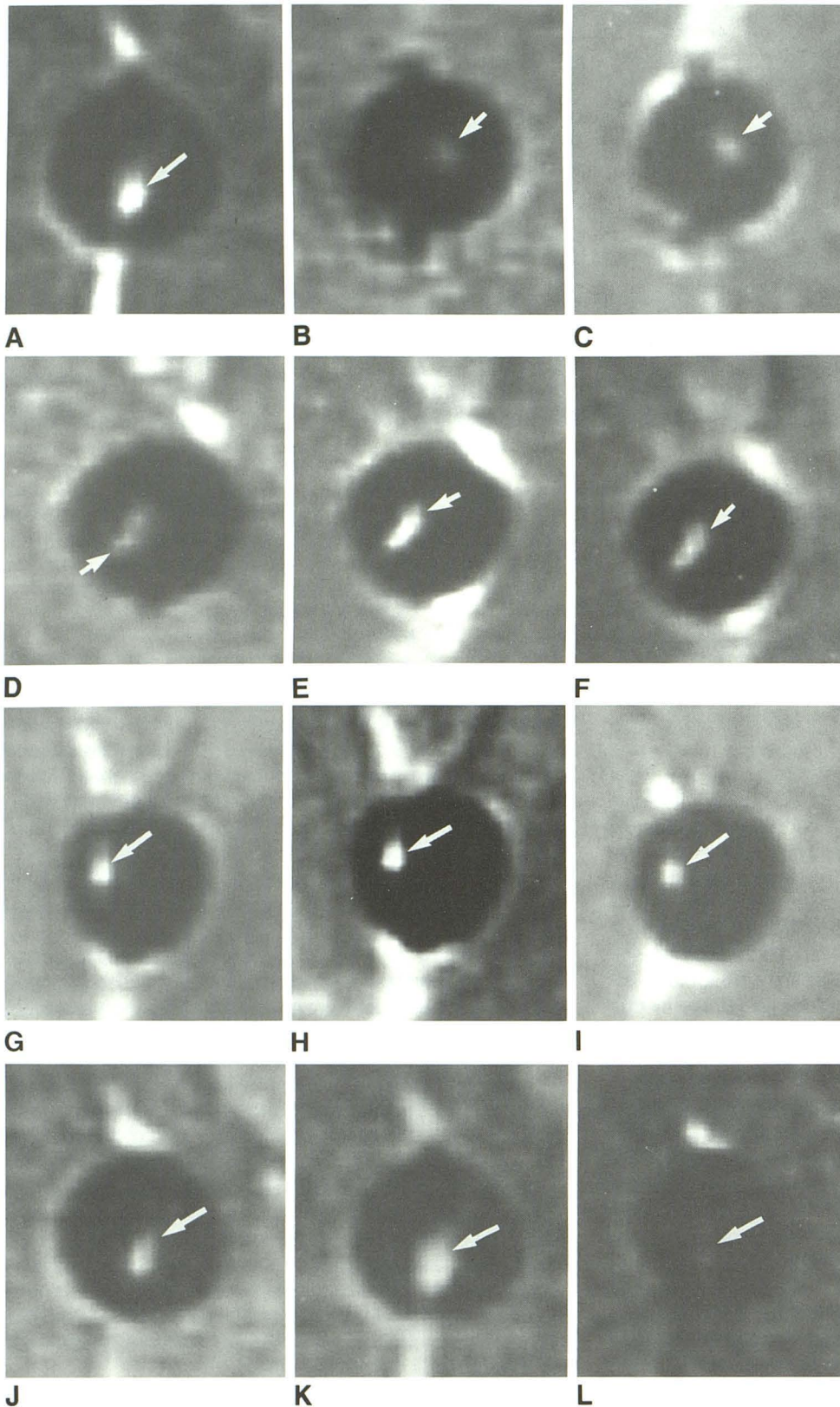


Fig. 2.—MR images of normal and demyelinated nerves.

A–C, Control nerve.

A, SE 500/28. Nerve is seen as small, rounded region of intermediate signal intensity (arrow), similar to muscle, surrounded by circular area of low signal intensity produced by silicone chamber.

B, SE 2000/56, heavily T2-weighted image. Nerve (arrow) appears similar to that seen on relatively T1-weighted sequence (A).

C, IR 1000/300/30, heavily T1-weighted image. Nerve (arrow) appears to be of slightly higher intensity than muscle, and brighter than on relatively T1-weighted (A) and heavily T2-weighted (B) sequences.

D–F, Category 1 nerve.

D, SE 500/28, relatively T1-weighted image. Nerve (arrow) shows no perceptible signal change.

E, SE 2000/56, heavily T2-weighted image. Nerve (arrow) shows marked increase in signal intensity.

F, IR 1000/300/30, heavily T1-weighted image. Nerve (arrow) appears to be of slightly higher intensity than muscle, not unlike control nerve.

G–I, Category 2 nerve.

G, SE 500/28, relatively T1-weighted image. Nerve (arrow) shows slight increase in signal intensity.

H, SE 2000/56, heavily T2-weighted image. Nerve (arrow) shows marked increase in signal intensity.

I, IR 1000/300/30, heavily T1-weighted image. Nerve (arrow) is of slightly higher intensity than muscle, not unlike control nerve.

J–L, Category 3 nerve.

J, SE 500/28, relatively T1-weighted image. Nerve (arrow) shows slight increase in signal intensity.

K, SE 2000/56 heavily T2-weighted image. Nerve (arrow) shows marked increase in signal intensity.

L, IR 1000/300/30, heavily T1-weighted image. Nerve (arrow) shows marked decrease in signal intensity.

**Fig. 3.—Nerve histology.**  
**A, and B, Control nerve.**  
**A, Myelin stain (×10).** Myelin sheaths appear normal (*arrow*).  
**B, Corresponding section stained for thionin (×10)** shows a normal number of glial cells (*arrow*).  
**C and D, Category 1 nerve.**  
**C, Myelin stain (×10)** shows beading of myelin (*arrowhead*) around most axon cylinders and nearly complete absence of myelin in others (*arrow*).  
**D, Corresponding section stained for thionin (×50).** Nerve shows a twofold increase in number of glial elements (*arrowhead*).  
**E and F, Category 2 nerve.**  
**E, Myelin stain (×10)** shows scattered dark-staining myelin debris.  
**F, Corresponding section stained for thionin (×100)** shows twofold increase in number of glial elements (*arrow*).  
**G and H, Category 3 nerve.**  
**G, Myelin stain (×100)** shows scattered, dark-staining myelin debris (*arrow*).  
**H, Corresponding section stained for thionin (×100)** shows fourfold increase in number of glial elements.

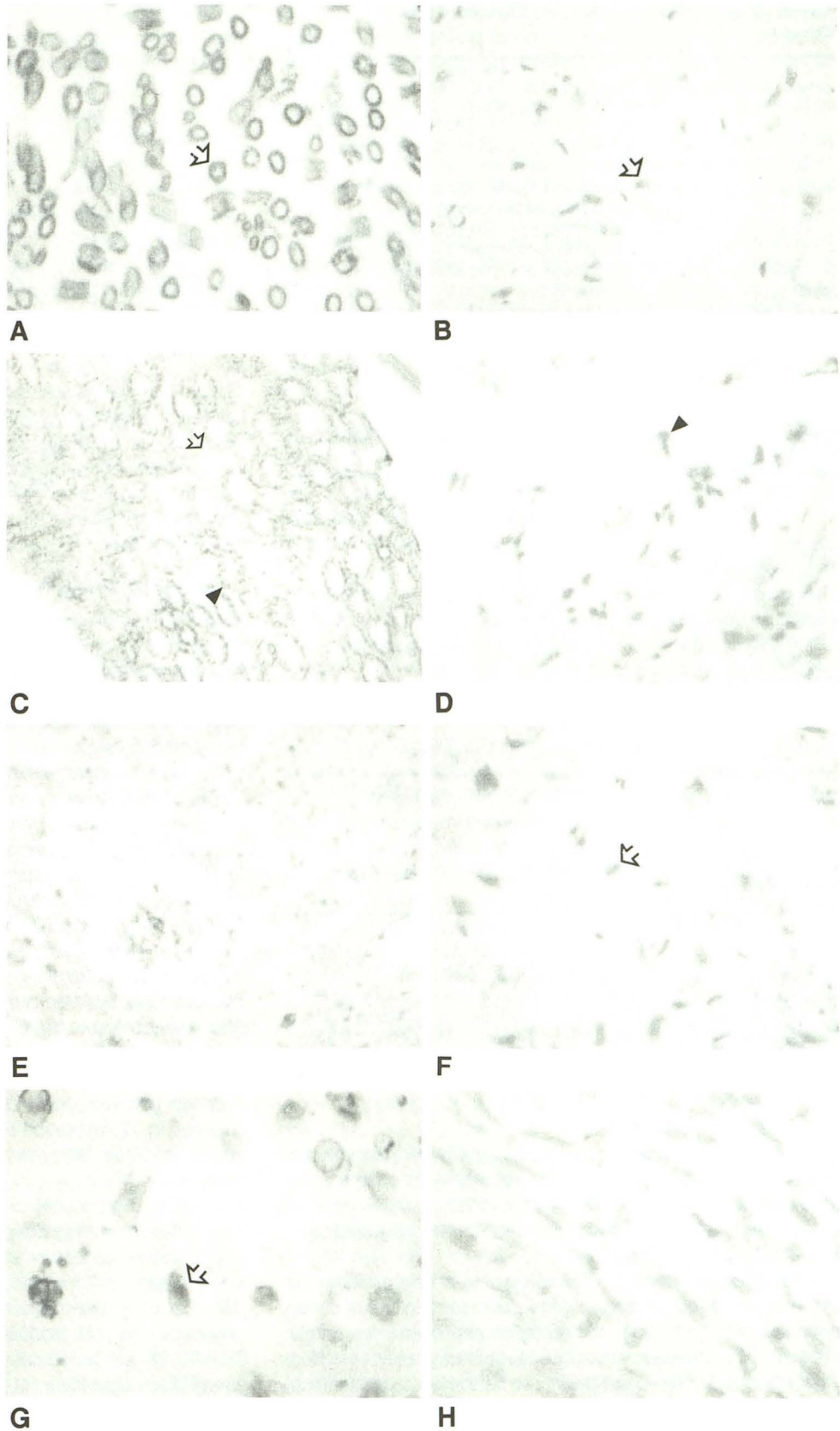


**TABLE 1: Categories of Histologic Changes with Myelin and Thionin**

Category	Change
1: Myelin	Beading and fragmentation of myelin around most axon cylinders and some axon cylinders showing complete loss of myelin
Glial elements	Doubled relative to control
2: Myelin	Further loss of myelin with only scattered myelin fragments present
Glial elements	No perceptible increase in the number of glial elements compared with category 1
3: Myelin	No further loss of myelin compared with category 2
Glial elements	More than a fourfold increase compared with control nerves

**TABLE 2: Categorization of Nerve Segments by Histologic Changes**

Injury: Location	Histologic Category		
	1	2	3
Crush (n = 7):			
Proximal	4	3	0
Distal	0	2	5
Transection (n = 5):			
Proximal	2	3	0
Distal	0	1	4
Alcohol (n = 5):			
Proximal	0	0	5
Distal	0	0	5
Total	6	9	19

Note.—Categories of histologic changes are described in Table 1.

**TABLE 3: Changes in Relative Signal Intensity by Histologic Categories**

Sequence	Mean Signal Intensity ± Absolute Range		
	Category 1	Category 2	Category 3
SE 500/28	1.08 ± 0.12	1.28 ± 0.14	1.10 ± 0.09
SE 2000/56	1.61 ± 0.11	1.94 ± 0.23	2.26 ± 0.31
IR 1000/300/30	0.94 ± 0.14	1.06 ± 0.12	0.54 ± 0.15

Note.—Categories of histologic changes are described in Table 1.

cholesterol, glycosphingolipid, and sphingomyelin) disappears rapidly and at a similar rate. Cholesterol ester is seen for the first time. When breakdown and resorption of myelin debris is complete, cell multiplication ceases. Total cell population may reach eight times normal.

After 30 days (stage 3), the cytoplasm of the proliferated and hypertrophied neuroglial cells decreases in volume, resulting in the formation of neuroglial cell bands intimately covered by endoneurial sheaths. Nucleic acid concentration returns toward normal and the nerve fibril shows volume loss and fibrosis.

It must be emphasized that studies of the chemistry of degeneration generally involve analyses of the whole nerve.

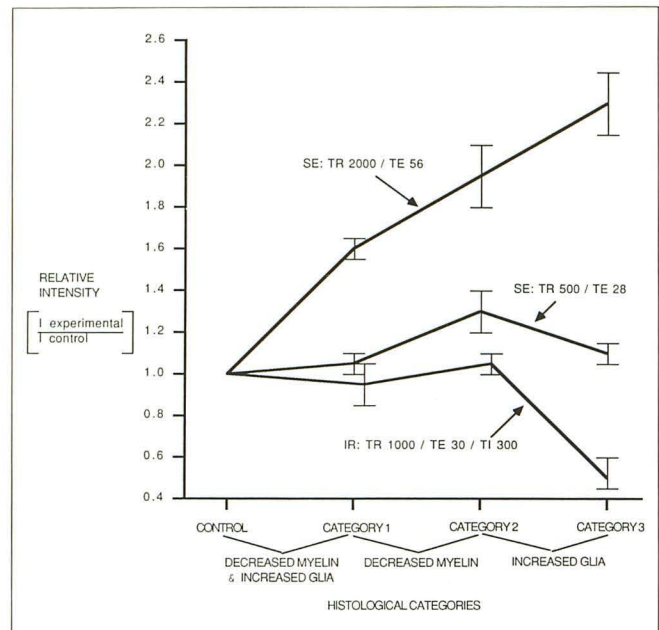


**Fig. 4.—Plot of changes in relative signal intensity by histologic categories.**

Results, therefore, represent the combined chemical constituents of all structures of the peripheral nerve—axon, myelin, neurilemma, macrophages, collagenous fibers, and other connective tissue elements. Chemical studies on individual components are not yet feasible technically.

The three histologic categories of nerve in our study, therefore, were consistent with evolving phases of stage 2 degeneration. Category 1 nerves exhibited beading and fragmentation of myelin around most axon cylinders with some axon cylinders showing complete loss of myelin, associated with a doubling of glial elements (Figs. 3C and 3D). These nerves showed a marked increase in signal intensity on the T2-weighted SE 2000/56 sequence, approximately 1.5 times that of respective control nerves. Relatively T1-weighted SE 500/28 sequences and heavily T1-weighted IR 1000/300/30 sequences showed no significant signal change. Thus, images of nerves undergoing early demyelination and neuroglial proliferation showed signal changes consistent with significant changes in T2 relaxation time. Signal changes may be attributable to either demyelination or neuroglial proliferation or both.

The fact that signal changes were appreciated only on heavily T2-weighted sequence is of interest. It is unlikely that a significant increase in T2 is unaccompanied by a concomitant increase in T1 in the absence of a paramagnetic effect [10]. Certainly, there is a significant contribution of T2 relaxation to the signal produced with the relatively T1-weighted SE 500/28 sequence. IR sequences, however, are usually purely T1-weighted. In current imaging protocols, however, most IR sequences use a second 180° refocusing pulse to increase readable signal, inducing minimal, but perhaps not insignificant, T2-weighting to the images. Our IR sequence

uses such a refocusing pulse and a TE of 30. Thus, it is likely that marked changes in T2 relaxation mask the contributions of changes in T1 relaxation to the signal, even in this heavily T1-weighted sequence.

Category 2 was characterized by further loss of myelin with only scattered myelin fragments present. In these nerves there was no perceptible increase in the number of glial elements compared with category 1 (Figs. 3E and 3F). These nerves showed further increase in relative signal intensity on the heavily T2-weighted SE 2000/56 sequence compared with category 1 nerves. Unlike category 1 nerves, category 2 nerves showed a moderate increase in signal intensity on the relatively T1-weighted SE 500/28 sequence. Category 2 nerves showed no change in relative signal intensity on the heavily T1-weighted IR 1000/300/30 sequence.

When compared with category 1 nerves, category 2 nerves, therefore, show that there is a change in MR signal intensity with loss of myelin alone, not attributable to a neuroglial proliferation. Again, the further marked increase observed in T2 may account for the moderate increase in signal on the relatively T1-weighted SE sequence and the absence of perceptible signal change on the heavily T1-weighted IR sequence.

Category 3 nerves showed no further loss of myelin; however, there was a more than twofold increase in glial elements compared with category 2 nerves (Figs. 3G and 3H). Category 3 nerves demonstrated an even further increase in relative signal intensity over category 2 nerves on the heavily T2-weighted SE 2000/56 sequence. Unlike category 2 nerves, category 3 nerves evidenced decreased signal intensity on the IR 1000/300/30 sequence. A slight increase in relative signal intensity was sometimes appreciated on the SE 500/28 sequence for category 3 nerves.

MR signal data in category 3 compared with category 2 nerves indicates an increase in both T1 and T2 relaxation times with increase in the number of glial elements alone, independent of the degree of demyelination. In category 3 nerves, despite the increase in signal on the heavily T2-weighted SE sequence, a decrease in signal is seen on the heavily T1-weighted IR sequence. This perceptible decrease in signal on the IR sequence, combined with the relatively insignificant change in signal on the relatively T1-weighted SE sequence, supports the contention that T2 effects dominate the MR signal from category 1 and 2 nerves, masking changes in T1 on conventional T1-weighted sequences.

It is known that the MR signals of myelinated nerves in imaging and relaxation studies are mainly due to water protons. Deuteron exchange experiments have shown that no significant contribution of lipid protons is present in relaxation signals of white matter [9]. Under the experimental conditions used, only water, hydroxyl, and amine protons will exchange with deuterons, which is consistent with the uniexponential decay observed in both T1 and T2 for deuteron-exchanged white matter. This observation is supported by the almost equal proton densities of white matter measured by MR and calculated from water content. The signals arising from lipid protons in white matter are only visible in high-resolution MR spectra after removing a part of the water protons by deuteron

exchange. Thus, the T1 and T2 of white matter mainly reflect the state of the water protons. The changes in signal intensity we observed in evolving demyelination, therefore, are best interpreted by considerations of the changes in nerve water associated with degeneration.

Studies of T2 relaxation times measured by high-resolution MR spectroscopy in the frog sciatic nerve have shown that there are three experimentally distinct compartments of water [10]. A slowly relaxing fraction, amounting to about 21% of the total tissue water, is probably located in the intercellular space, representing the extracellular water. The physical properties of this fraction are the closest to those of a dilute aqueous solution; however, the propinquity to macromolecular surfaces lowers its transverse relaxation time. The fast relaxing component, representing about 29% of the signal, may be ascribed to water closely associated with the proteins and phospholipids of the myelin membrane, having the physical properties strongly affected by this association. The intermediate relaxation time fraction, amounting to about 50% of the whole nerve water, most probably represents the axoplasmic water.

Axonal membranes and myelin surfaces constitute barriers for tissue water protons, creating different macromolecular environments [11, 12]. It has been shown that proton MR relaxation characteristics of body tissue are related to water-surface interactions, and it appears that the tissues with the shorter relaxation times contain an abundance of surfaces, primarily in the form of membranes [11]. Similarly, myelin may not only significantly restrict the motion of water within and upon the membrane itself, but also limit the rate of water exchange between intraaxonal and extraaxonal compartments. Thus, it is conceivable that the process of demyelination and axonal degeneration alters the physical state and compartmentalization of water in the nerve fibers. With demyelination there would be a decrease in membrane-bound water, characterized by a short relaxation time, and a concomitant increase in extracellular water, characterized by a longer relaxation time.

Certainly an increase in absolute nerve water would also produce longer relaxation times. It is known, however, that absolute nerve water associated with demyelination is closely correlated with the number of neuroglial cells [7, 13]. Thus, signal changes observed between our histologic categories 1 and 2, in which there was no change in the number of glial cells, are not well explained by an increase in total water content and are best explained by changes in the physical state and compartmentalization of water. On the other hand, signal changes observed between our histologic categories 2 and 3, in which there was a fourfold increase in the number of glial cells and no change in the appearance of myelin, may be attributable to an increase in the total water content of the nerve.

We cannot yet fully appreciate how specific changes in the quantity, physical state, and compartmentalization of water in the demyelinated nerve influences signal characteristics. This study, however, has yielded two fundamental observations: (1) perceptible signal changes associated with early nerve degeneration, in which there is demyelination in the

absence of glial cell proliferation, are appreciated as increased intensity on heavily T2-weighted sequences and (2) perceptible signal changes associated with more progressive nerve degeneration, in which there is an increase in the number of glial cells in the absence of further demyelination, are appreciated as decreased intensity on T1-weighted sequences and increased intensity on T2-weighted sequences, respectively. The ability of MR to distinguish evolving changes in degenerating nerves provides a powerful method for diagnosing demyelinating disease in both the central and peripheral nervous systems.

#### REFERENCES

1. Jolesz FA, Polak JF, Adams DF, Ruenzel PW. Myelinated and nonmyelinated nerves: comparison of proton MR properties. *Radiology* **1987**;164:89-91
2. Jolesz F, Polak J, Ruenzel P, et al. Wallerian degeneration demonstrated by magnetic resonance: spectroscopic measurements on peripheral nerve. *Radiology* **1983**;149:345-348
3. Lukes SA, Crooks LE, Aminoff MJ, et al. Nuclear magnetic resonance imaging in multiple sclerosis. *Ann Neurol* **1983**;13:592-601
4. Misra L, Egan W, Vijeswarapu J, et al. Early detection of diabetic neuropathy by NMR relaxation times. Presented at the annual meeting of the Society of Magnetic Resonance Imaging in Medicine, Montreal, Canada, March **1986**
5. Cobb SR, Mehringer CM. Wallerian degeneration in a patient with Schilder disease: MR imaging demonstration. *Radiology* **1987**;162:521-522
6. Rossiter RJ. The chemistry of Wallerian degeneration. In: Folch-Pi, ed. *Chemical pathology of the nervous system*. New York: Pergamon, **1961**:207-227
7. McCaman RE, Robins E. Quantitative biochemical studies of Wallerian degeneration in the peripheral and central nervous systems. I. Chemical constituents. *J Neurochem* **1959**;5:18-31
8. Bottomley PA, Hart HR, Edelstein WA, et al. Anatomy and metabolism of the normal human brain studied by magnetic resonance at 1.5 Tesla. *Radiology* **1984**;150:441-446
9. Kamman RL, Go KG, Muskiet FAJ, Stomp GP, Van Dijk P, Berendson HJK. Proton spin relaxation studies of fatty tissue and cerebral white matter. *Magn Reson Imaging* **1984**;2:211-220
10. Vasilescu V, Katona E, Simplaceau V, Demco D. Water compartments in the myelinated nerve. III. Pulsed NMR results. *Experientia* **1978**;34:1443-1444
11. Cameron IL, Ord VA, Fullerton GD. Characterization of proton NMR relaxation times in normal and pathological tissues by correlation with other tissue parameters. *Magn Reson Imaging* **1984**;2:97-106
12. Jenkinson TJ, Kamat VB, Chapman D. Physical studies of myelin. II. Proton magnetic resonance and infrared spectroscopy. *Biochim Biophys Acta* **1969**;183:427-433
13. Hirose G, Bass NH. A quantitative histochemical study of early cellular events associated with destruction of myelinated axons in rat optic nerve. *Exp Neurol* **1974**;44:82-95